Vehicle System Dynamics, Vol 36, No.4-5, November 2001, pp.359-389

Differential-Braking-Based Rollover Prevention for Sport Utility Vehicles with Human-in-the-loop Evaluations

BO-CHIUAN CHEN[1] and HUEI PENG[2]

SUMMARY

An anti-rollover control algorithm based on the Time-To-Rollover (TTR) metric is proposed in this paper. A simple model with steering and direct yaw moment control inputs was constructed to calculate the TTR in real-time. The TruckSim dynamic simulation software was used to verify the control performance, as well as to simulate the system dynamics in the UM-Oakland driving simulator. Both the simple and complex (TruckSim) models were tuned to match the behavior of a 1997 Jeep Cherokee vehicle with lateral acceleration up to 0.6g. The performance of the proposed control system was compared with other threshold-based rollover-prevention control algorithms. Finally, a human-in-the-loop experiment was conducted to study the performance of the proposed algorithm under more realistic driving conditions.

1. INTRODUCTION

In the U.S., more than 35,000 people were killed in road accidents each year from 1993 to 1998 [1]. Among them, about 10% were the result of non-collision crashes. Reports also showed that rollover was involved in about 90% of the first harmful events of non-collision fatal crashes. Furthermore, the average percentage of rollover occurrence in fatal crashes was significantly higher than in other types of crashes. Compared to other types of vehicles, Sport Utility Vehicles (SUV) had the highest rollover rates. Due to the increasing popularity of SUVs, the percentage of fatal rollover crashes in which at least one SUV was involved also increased significantly from 1993 to 1998. Because SUVs are more prone to rollover compared to passenger vehicles, the federal government issued an upgraded rollover warning label in 1999 [2], which is now required to be displayed on all new SUVs.

SUVs are constructed with higher ground clearance, which is the main reason for their higher rollover rate. In order to help consumers understand a vehicle's likelihood to roll over, Secretary Rodney Slater and Deputy Administrator Rosalyn Millman of the National Highway Traffic Safety Administration (NHTSA) proposed a rollover rating program [3]. For passenger cars, the star rating range is between 4 and 5 stars. For SUVs, the range is between 1 and 3 stars because of their higher center of gravity (CG).

Rollover prevention can be achieved by employing rollover warning and anti-rollover systems. Most existing rollover warning systems [4,5,6,7,8,9,10] are based on signal threshold techniques. These systems turn on the warning actions when the vehicle roll angle or the lateral acceleration exceeds a pre-selected threshold value. They are usually conservative and do not predict impending rollover danger in the future, which is very important for drivers to correct the dangerous maneuver and avoid the rollover accident before the threshold value is exceeded. To prevent/reduce rollover, one of the most important enabling techniques is the development of accurate rollover threat indices. A rollover warning/control algorithm will work well only if the impending vehicle rollover threat can be accurately represented. The authors proposed a Time-To-Rollover (TTR) metric [11,12] for rollover prevention. In theory, TTR provides a better assessment of impending rollover threat, and thus could be the basis for rollover warning and anti-rollover control algorithms. In [11], it was shown that the TTR for SUVs is too short for human drivers to respond. It is an indication that an active control may be necessary to assist drivers for rollover prevention.

Four types of actuation mechanisms were proposed in the literature for rollover reduction, i.e. four wheel steering, active suspension, active stabilizer, and differential braking. Furleigh et al. [13] proposed multiple steered axles for articulated heavy trucks. The tractor has 1 front steering axle and 2 rear axles. Their algorithm assumes the steering at the rear axles is proportional to the

[1] Graduate Student

[2] Associate Professor, Department of Mechanical Engineering, University of Michigan, Ann Arbor, MI 48109-2125, U.S.A. Tel. (734) 936-0352, E-mail: hpeng@umich.edu.

front steering angle. The proportional gain is defined as a function of vehicle forward speed. The lateral acceleration of the trailer can be reduced at high-speed obstacle avoidance maneuvers. Dunwoody [14] proposed an active roll control system consisting of a hydraulic fifth wheel and active suspension to control the roll motion of the vehicle. It can raise the static rollover threshold by 20-30%. Lin et al. [15,16,17] proposed a roll control system based on active suspension and lateral acceleration feedback for single-unit and articulated trucks. Their control system was found to reduce the transient and steady state load transfer for a range of maneuvers and increase the rollover safety of the vehicle. Sampson [18] proposed a more systematic control design by using state feedback and LQR techniques. Parsons et al. [19] developed the Active Cornering Enhancement (ACE) system and implemented it on the new Land Rover Discovery vehicles. ACE utilizes the active stabilizer to generate torques between the front/rear axle and the vehicle body when the vehicle is turning. The roll angle is reduced and the rollover threshold is thus increased. Konik et al. [20] developed a new active roll stabilization system named "Dynamic Drive." Dynamic Drive utilizes an active stabilizer for active torque distribution between front and rear axles according to different driving conditions. Similar to ACE, the roll motion is reduced and the rollover threshold is increased. Palkovics et al. [21,22] proposed a Roll-Over Prevention (ROP®) system for commercial vehicles. They utilized measurements of the wheel speed and the lateral acceleration to estimate wheel lift-off. If wheel lift-off is detected by estimation, ROP® will activate full brake application of the vehicle. Wielenga [23,24] proposed Anti-Rollover Braking (ARB) by using differential braking instead of full brake application. They utilized the rebound bumpers to detect tire lift-off. Rebound bumper contact occurs just before the tire lift-off. Whenever the tire lift-off is detected or the lateral acceleration of the vehicle is larger than the threshold value, ARB will activate differential braking.

We propose an anti-rollover control algorithm that is based on the TTR metric in this paper and differential braking is selected as the control actuator because: (1) Four wheel steering, active suspension, and active stabilizer are not only expensive but also difficult to implement in the existing vehicle schemes. In contrast, differential braking has lower cost and is already available for Vehicle Dynamic/Stability Control (VDC/VSC) systems. (2) Differential braking is considered the most effective way to manipulate tire force to reduce the lateral acceleration of the vehicle. (3) The forward speed contributes to the lateral acceleration of the vehicle. Differential braking can reduce the forward speed that cannot be reduced by four wheel steering, active suspension, and active stabilizer. The proposed control algorithm will activate differential braking if the TTR is less than a preset value, for example, 0.5 sec. Preliminary results show that this provides superior performance to control algorithms based on threshold values of lateral acceleration or roll angle.

Many active safety systems are designed without considering driver interaction. The driver's interaction with and perception of the system performance may pose a problem. Although in general a driver may gradually adapt to the active safety system and change his/her behavior, the performance of the human-in-the-loop system is not guaranteed and needs to be studied carefully. The performance of the proposed TTR-based anti-rollover control algorithm (which has been designed through simulations) will be studied using the UM-Oakland driving simulator made available to us by the Oakland University [25].

The remainder of this paper is organized as follows: a brief review of the Time-To-Rollover metrics is presented in Section 2. In Section 3, the TTR-based anti-rollover control algorithm is defined and presented. The optimization procedure of the control gain is presented in Section 4. Test conditions and results of a human-in-the-loop evaluation study are presented in Section 5. Finally, conclusions are made in Section 6.

2. TIME-TO-ROLLOVER METRICS

Tire lift-off is defined as the unacceptable rollover event in this paper. To be more precise, the term "Time-To-Rollover" actually means "Time-To-Tire-lift-off." This definition will not result in any major change in the overall algorithm development. A more aggressive or conservative roll event definition can be used and the design process to be described below will remain the same.

After a "rollover" (tire-lift-off) has occurred, a true-TTR can be computed in an after-thought manner. In other words, whenever the vehicle roll angle exceeds the defined threshold value, we can roll back the clock and define a point 0.2 sec before this rollover incident to have a "true-TTR" of 0.2 sec. This is like drawing a straight line with slope –1 on the time-TTR plot from the rollover instant (see Fig. 1). Ideally, if we can re-construct the TTR in real-time and in a predictive manner, the severity of the rollover threat can be accurately represented and reported. Based on the TTR metric, various warning/control systems can be designed.

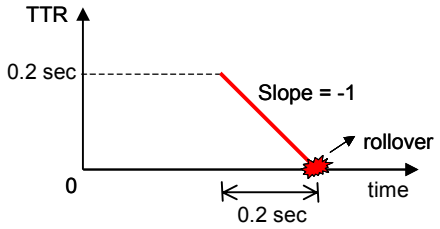

Fig. 1. TTR notion.

A model-based TTR is defined as follows: assuming the input steering angle stays fixed at its current level in the foreseeable future, the time it takes for the vehicle sprung mass to reach its critical roll angle is defined as the (model predicted) TTR. Motion prediction techniques were used to help develop the vehicle model for predicting the future roll angle.

The flow chart of the TTR calculation algorithm is shown in Fig. 2. The vehicle model takes the necessary initial conditions and driver's steering input, and the algorithm integrates the model for up to X sec into the future, by assuming constant steering during the integration time horizon. Under normal driving conditions, the model predicted TTR is usually very large and may even approach infinity. For example, if the driver is driving straight, there is no roll motion at all. Therefore, the TTR is approaching infinity. For implementation considerations, we can saturate the model predicted TTR at X sec. In other words, we will only integrate the vehicle model for up to X sec. If it is found that the vehicle does not roll over, the model-predicted TTR is said to be X sec. The roll angle threshold can be specified differently for different vehicles, or for different aggressiveness of roll motion predictions.

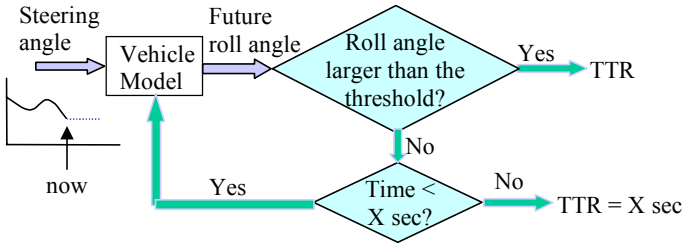

Fig. 2. Flow chart of the TTR calculation algorithm.

The vehicle model can be either a nonlinear complex or a linear simple model. In order to predict a TTR of (up to) 0.5 sec, one needs to predict vehicle response in the next 0.5 sec repeatedly. If TTR is updated every 10 ms, the vehicle model needs to be 50 times faster than real-time. Therefore, we can only afford to use the simple model to calculate the TTR metric. A 3DOF yaw-roll model [26] is used as the simple model in this paper.

Vehicle parameters of a 1997 Jeep Cherokee published by Vehicle Research and Test Center (VRTC, located at East Liberty, OH) in [27] were used to construct the 3DOF model developed from the Lagrangian dynamics. The side view of the 3DOF yaw-roll model is shown in Fig. 3.

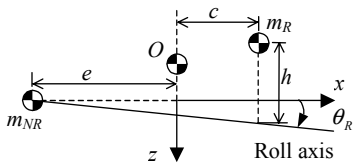

Fig. 3. Side view of the 3DOF yaw-roll model.

Where m_R is the rolling sprung mass and m_{NR} is the non-rolling unsprung mass. Point O is the overall CG of the model. The roll axis is pointing down with an angle θ_R with respect to the horizon plane. Equations of motion (EOM) in matrix form are shown in Eq.(1).

$$\begin{bmatrix} mu_0 & 0 & m_R h & 0 \\ 0 & I_z & I_{xz} & 0 \\ m_R h u_0 & I_{xz} & I_x & 0 \\ 0 & 0 & 0 & 1 \end{bmatrix} \begin{bmatrix} \dot{\beta} \\ \dot{r} \\ \dot{p} \\ \dot{\phi} \end{bmatrix} + \begin{bmatrix} -Y_\beta & mu_0 - Y_r & 0 & -Y_\phi \\ -N_\beta & -N_r & 0 & -N_\phi \\ 0 & m_R h u_0 & -L_p & -L_\phi \\ 0 & 0 & -1 & 0 \end{bmatrix} \begin{bmatrix} \beta \\ r \\ p \\ \phi \end{bmatrix} = \begin{bmatrix} Y_\delta \\ N_\delta \\ 0 \\ 0 \end{bmatrix} \delta_{tire} \qquad (1)$$

where β is the side slip angle of the vehicle, r is the yaw rate, p is the roll rate, and ϕ is the roll angle of the sprung mass. Parameters of the Jeep Cherokee were used to calculate the entries of the matrices of Eq.(1). Detailed descriptions of each entry in Eq.(1) are listed in Appendix 1. If we express Eq.(1) as Eq.(2),

$$E\dot{x} + Fx = G\delta_{tire} \qquad (2)$$

where $x = [\beta \quad r \quad p \quad \phi]^T$, the state space form of Eq.(2) is then

$$\dot{x} = Ax + B\delta_{tire} \qquad (3)$$

where $A = -E^{-1}F$ and $B = E^{-1}G$.

This model was obtained under the constant vehicle speed assumption. In order to predict the roll motion correctly, the model needs to be gain-scheduled with respect to the vehicle speed. The vehicle speed u_0 and those entries containing u_0 could be updated at every integration time step. We can integrate the state space Eq.(3) by using the ode2 integration method to predict the future roll angle of the sprung mass (see Fig. 2). After matching the 3DOF yaw-roll model with the Jeep Cherokee field test data (also obtained from VRTC), representative simulation responses are shown in Fig. 4 and 5. Since the root-mean-square (RMS) value of the roll-angle prediction error was only 0.1003 deg, the 3DOF model was determined to be satisfactory for roll motion prediction.

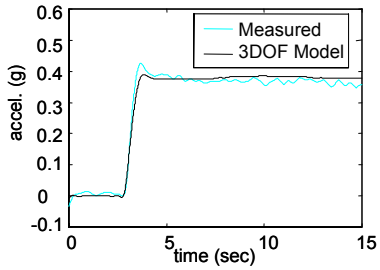

Fig. 4. Lateral acceleration prediction of the 3DOF yaw-roll model. (50 mph 0.4 g left turn).

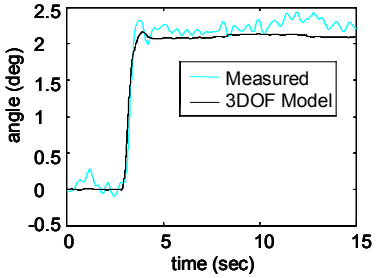

Fig. 5. Roll angle prediction of the 3DOF yaw-roll model (50 mph 0.4 g left turn).

3. ANTI-ROLLOVER CONTROL

3.1 Simulation Model

TruckSim [28] is the simulation model used for verifying the proposed anti-rollover control algorithm in this paper. TruckSim was a simulation program developed by the Engineering Research Division of the University of Michigan Transportation Research Institute. TruckSim has been commercialized and now can be licensed from the Mechanical Simulation Corporation (MSC). A Jeep Cherokee model was built using the parameters published by VRTC [27]. The TruckSim template we used is for a single unit vehicle with two axles. It includes a 14 DOF model with 37 state variables. The dynamic responses of the Cherokee model in TruckSim were verified by the vehicle test data of the 1997 Jeep Cherokee, which was also obtained from VRTC.

The maneuvers used for model verification were constant speed J turn and pulse steer under three steering levels (either right or left) directions at 25 and 50 mph, respectively. The lateral acceleration and roll angle responses of TruckSim under selected test conditions are shown in Fig. 6 and 7. The light gray solid lines represent 10 test runs under the specific maneuver type and the gray solid line represents one run selected from the 10 runs. The steering of the selected run was then input to TruckSim. The black dot line represents the response of the TruckSim model. As can be seen from Fig. 6 and 7, the lateral acceleration and roll angle responses of the TruckSim simulation agree with the test data.

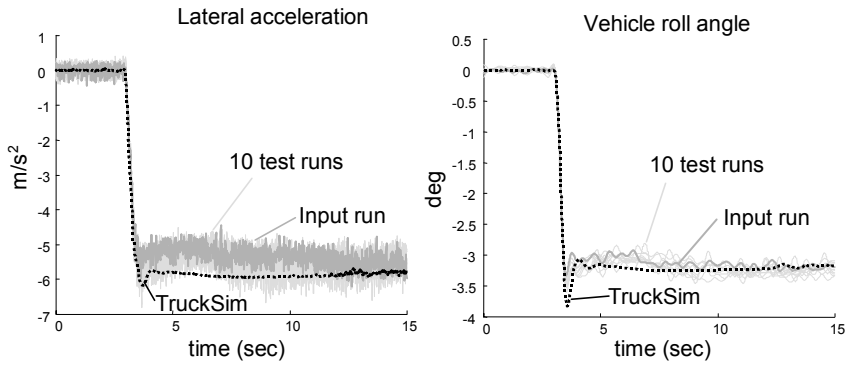

Fig. 6. Cherokee model response (25 mph right turn, 0.6g).

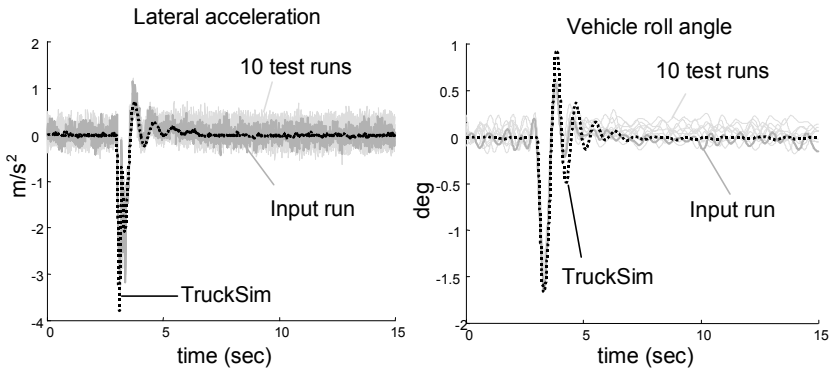

Fig. 7. Cherokee model response (50 mph pulse steer right turn).

The RMS values of the lateral acceleration and roll angle response errors of TruckSim are listed in Table 1. Since the responses of TruckSim have been verified against test data with lateral acceleration level of up to 0.6g, TruckSim will be viewed as a full nonlinear complex model accurately representing the Cherokee vehicle.

Table 1. RMS values of lateral acceleration and roll angle response errors of TruckSim compared to the vehicle test data of 1997 Jeep Cherokee.

	RMS value
Lateral Acceleration	0.372 m/s^2 (0.0379 g)
Roll Angle	0.2130 deg

3.2 TTR-based Anti-rollover Control Scheme

As mentioned in Section 1, differential braking is already available for VDC/ VSC systems and considered the most effective way to manipulate tire force to reduce the lateral acceleration of the vehicle. Therefore, differential braking is chosen as the actuator for the TTR-based anti-rollover control proposed in this paper. The effects of differential braking on anti-rollover control are shown in Fig. 8.

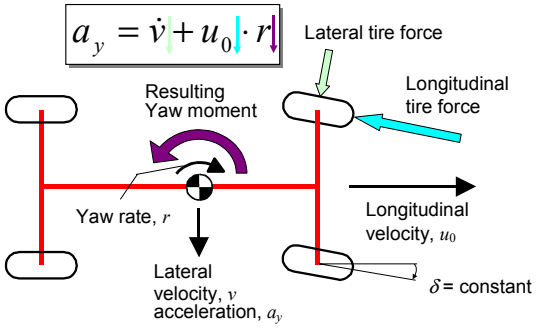

Fig. 8. Effects of differential braking.

By activating differential braking, a braking moment is applied to the front-outer wheel while the vehicle is turning. When a braking moment is applied to the wheel, its tire slip ratio changes. As can be seen from Fig. 9, the longitudinal braking force results from non-zero tire slip ratio. Therefore, the longitudinal velocity u_0 can be reduced by the longitudinal braking force.

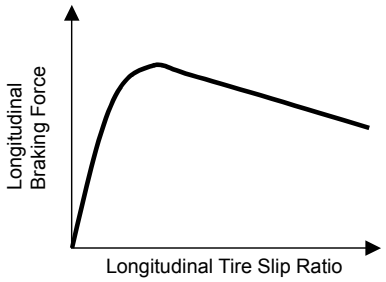

Fig. 9. Variation of longitudinal braking force with longitudinal tire slip ratio.

From the friction ellipse (shown in Fig. 10) concept [26], we know that the maximum lateral tire fore is determined by a given longitudinal tire force. Since the magnitude of the longitudinal braking force F_x is increased because of the applied braking moment, the lateral tire force F_y is consequently reduced. Therefore, the derivative of lateral velocity $\dot{v}$ is reduced by the reduced lateral tire force. The yaw moment resulting from the increased longitudinal braking force reduces the yaw rate r. It can be seen that we are reducing all three elements that contribute to the lateral acceleration a_y. The roll motion is excited mostly by the lateral acceleration. Therefore, the smaller the lateral acceleration is, the lower the rollover danger.

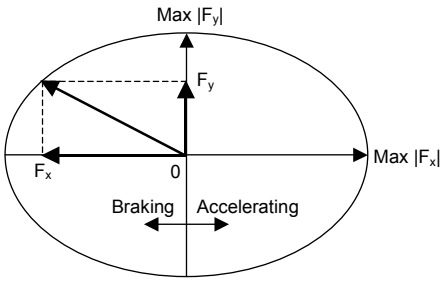

Fig. 10. Friction ellipse concept.

Existing anti-rollover systems (e.g., ARB system [23,24]) usually trigger the control action based on tire lift-off or lateral acceleration threshold. We propose to activate the control action by using the TTR metric because of its predictive nature. The proposed control scheme is shown in Fig. 11.

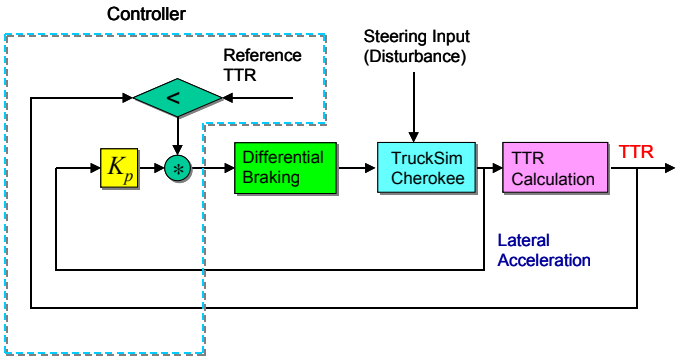

Fig. 11. TTR-based anti-rollover control scheme.

In Fig. 11, a Jeep Cherokee model in TruckSim is used for the verifications of the proposed anti-rollover control algorithm. In order to simplify the problem, the driver's steering input is viewed as the only disturbance to the vehicle (i.e. no braking from the driver). The reference TTR

is set to be the maximum TTR value, which is equal to the foreseeable X sec. in Fig. 2. In this paper, the reference TTR is set to be 0.5 sec and the roll angle threshold used for calculating the model predicted TTR is set to be 3 deg.

Differential braking controls the yaw motion of the vehicle by applying a braking moment on either the right or left wheel of the front axle. The control goal is to make the vehicle more understeer to reduce the rollover threat. It is also the reason that we didn't choose full braking as the control actuator. The yaw moment change by braking force for each wheel is shown in Fig. 12 [29]. As can be seen from Fig. 12, the full braking might have some combinations of braking forces that make the vehicle understeer less or even oversteer, which is not desired for reducing the lateral acceleration.

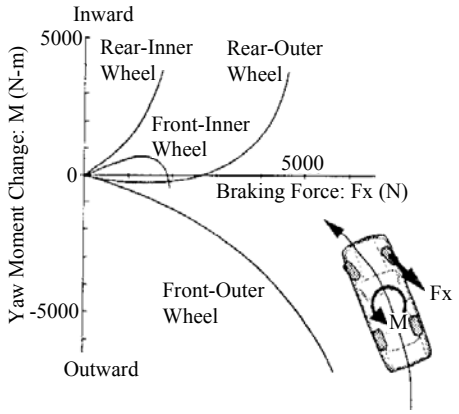

Fig. 12. Yaw moment change by braking force for each wheel [29].

Either lateral acceleration or roll angle can be selected for feedback control signal. The root-locus technique was used to help analyze both feedback control schemes. After the analysis, the lateral acceleration was chosen for the proportional feedback control design. Detailed design analysis and implementation process will be presented in Section 3.3.

Differential braking is implemented through the direct yaw moment control (shown in Fig. 13). The direct yaw moment control commands the anti-lock braking system (ABS) to generate the desired yaw moment. It interprets the desired yaw moment as the desired longitudinal braking force on either right or left front wheel. The desired longitudinal braking force is then interpreted as the desired tire slip ratio for ABS through a 2-dimenional look-up tire table. The look-up table takes the tire vertical load and the desired longitudinal force as inputs and generates the desired tire slip ratio as an output. ABS then controls the tire slip ratio by the brake system.

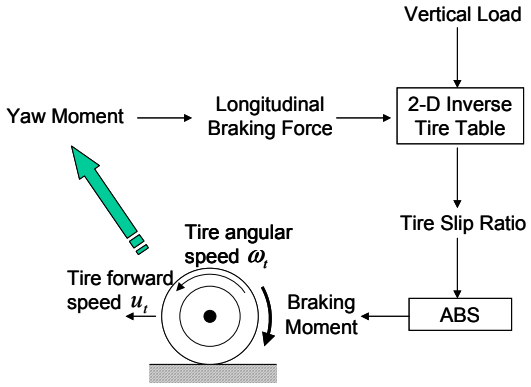

Fig. 13. Direct yaw moment control.

3.3 Feedback Control Design

In order to implement the direct yaw moment control, we need modify the 3DOF model to include the direct yaw moment control M_z as one of the inputs. The modified EOM of Eq.(1) is shown as

$$\begin{bmatrix} mu_0 & 0 & m_R h & 0 \\ 0 & I_z & I_{xz} & 0 \\ m_R h u_0 & I_{xz} & I_x & 0 \\ 0 & 0 & 0 & 1 \end{bmatrix} \begin{bmatrix} \dot{\beta} \\ \dot{r} \\ \dot{p} \\ \dot{\phi} \end{bmatrix} + \begin{bmatrix} -Y_\beta & mu_0 - Y_r & 0 & -Y_\phi \\ -N_\beta & -N_r & 0 & -N_\phi \\ 0 & m_R h u_0 & -L_p & -L_\phi \\ 0 & 0 & -1 & 0 \end{bmatrix} \begin{bmatrix} \beta \\ r \\ p \\ \phi \end{bmatrix} = \begin{bmatrix} Y_\delta \\ N_\delta \\ 0 \\ 0 \end{bmatrix} \delta_{tire} + \begin{bmatrix} 0 \\ 1 \\ 0 \\ 0 \end{bmatrix} M_z \tag{4}$$

If we express Eq.(4) as Eq.(5),

$$E\dot{x} + Fx = G_u u + G_d d \tag{5}$$

where $G_u = [Y_\delta \quad N_\delta \quad 0 \quad 0]^T$, $G_d = [0 \quad 1 \quad 0 \quad 0]^T$, $u = M_z$, and $d = \delta_{tire}$, we can obtain the state space equation as:

$$\dot{x} = Ax + B_u u + B_d d \tag{6}$$

where $A = -E^{-1}F$, $B_u = E^{-1}G_u$, and $B_d = E^{-1}G_d$. The subscripts u and d in Eqs.(5) and (6) denote for the direct yaw moment control and steering disturbance (as mentioned in Section 2, the steering is viewed as the disturbance to the system), respectively. The 3DOF model in Eq.(6) was used as the simple model for the TTR calculation throughout the anti-rollover control design.
After we have the TTR metric that is obtained by integrating the 3DOF model, we can design the feedback control for differential braking. Both lateral acceleration and roll angle feedback are analyzed in this subsection. The 3DOF model with the brake dynamics was viewed as the linearized Jeep Cherokee model and was used to design the proportional control gain by using the root-locus technique. The brake dynamics were approximated by a first order system with a time constant of 0.2 seconds in continuous time domain (shown in Eq.(7)).

$$\text{Brake dynamics} = \frac{1}{0.2s+1} \tag{7}$$

To simplify the problem, we started with the simple proportional control design. The block diagram of the closed loop system including the actuator dynamics is shown in Fig. 14.

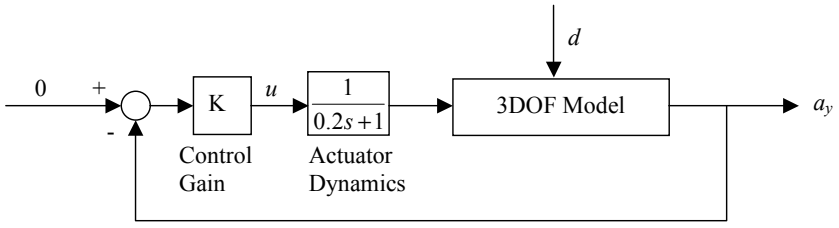

Fig. 14. Block diagram of the control design by lateral acceleration feedback with the 3DOF model.

In Fig. 14, K is the proportional control gain, u is the yaw moment input M_z, d is the steering input δ_{tire}, and a_y is the lateral acceleration. The details of the sub-loop ABS control were omitted here by assuming its time constant was much faster than that of the actuator dynamics. As

can be seen from Fig. 14, this was a regulation problem because the reference input was set to be zero and the control was trying to reject the disturbance effect.

Fig. 15 shows the root locus plot of the closed loop system of Fig. 14 in the s-domain. The yaw-mode branches approach the imaginary axis when we increase the control gain K. This is mainly due to our control strategy: brake on the front-outer wheel while the vehicle is turning (i.e., we are trying to make the vehicle more understeer). The closer the two yaw-mode branches approach the imaginary axis, the more understeer the vehicle. The largest K can be selected before the yaw-mode branches cross the imaginary axis. The largest K decreases when the vehicle speed increases.

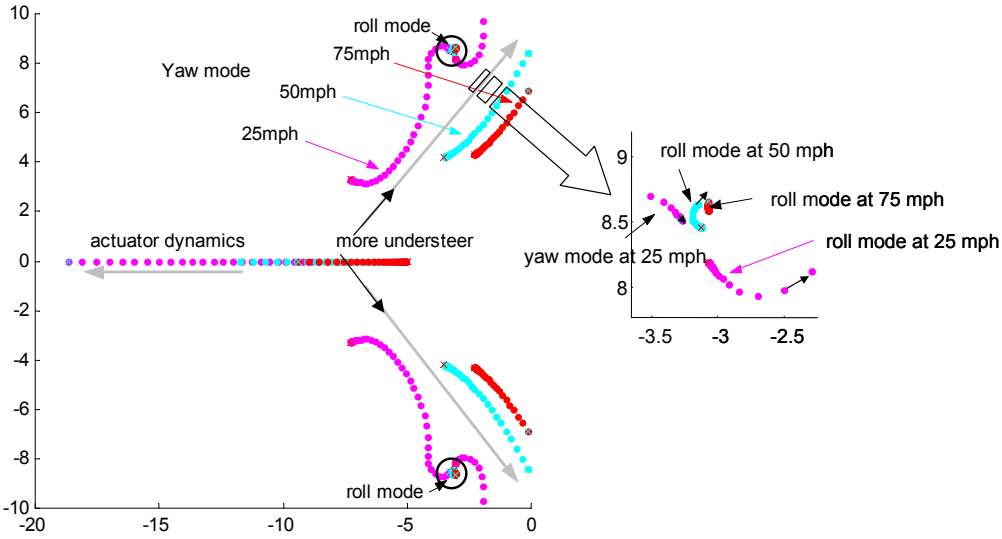

Fig. 15. Root locus plot of the closed loop system with lateral acceleration feedback in the s-domain.

The roll-mode branches are also shown in Fig. 15. As can be seen from the zoom-in plot of the circled part, the roll-mode branches at 25 and 50 mph move to the imaginary axis direction when we increase the control gain K. Therefore, we are making the vehicle less responsive to the steering disturbance. As for the yaw-mode branches at 75 mph, they barely move when we increase K (i.e., increasing K does not have much effect on the roll mode at high speeds).

If we replace the lateral acceleration a_y with the roll angle ϕ in Fig. 14, we can obtain the closed-loop system by feeding back the roll angle. The root locus plot of the resulting system in the s-domain is shown in Fig. 16. As can be seen from Fig. 16, the yaw-mode branches at 50 and 75 mph approach the imaginary axis when we increase the control gain K (i.e. more understeer). However, the yaw-mode branches at 25 mph move to the far left-hand-plane direction (i.e. less understeer) when K is too large.

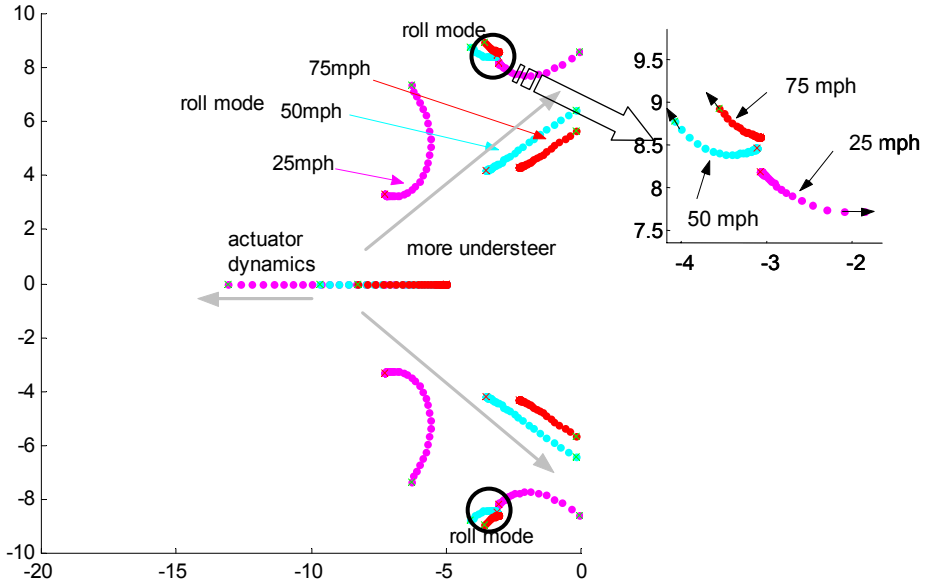

Fig. 16. Root locus plot of the closed loop system with roll angle feedback in the s-domain.

The roll-mode branches are also shown in Fig. 16. As can be seen from the zoom-in plot of the circled part, the roll-mode branches at 50 and 75 mph move to the left when we increase the control gain K. Therefore, we are making the vehicle more responsive to the steering disturbance. This makes the vehicle roll more than the open-loop system under the same steering disturbance.

Feeding back lateral acceleration gave us the desired and consistent root-locus pattern in both yaw and roll mode at all 3 design speeds. However, feeding back roll angle did not have a consistent root locus pattern at all 3 design speeds. In some cases as mentioned above, feeding back roll angle only made the system worse. Therefore, we chose to feed back lateral acceleration for the control design.

The control gain was not chosen by the root locus techniques. The root locus techniques were only used to help analyze the systems with the lateral acceleration and roll angle feedback. Since the driver closes the loop with the environment and the vehicle dynamics, the control gain of the anti-rollover control could be optimized using a driver model. The optimization process is presented in the following section.

4. OPTIMIZATION

4.1 Test Tracks

Test tracks for evaluating the anti-rollover control performance were designed based on the Man-Off-The-Street (MOTS) course [30]. Four parts of the MOTS course were selected and are shown in Fig. 17. The 1st test track is a large radius arc, the 2nd test track is an obstacle avoidance maneuver, the 3rd test track is a small radius arc instead of the original gravel turn, and the 4th test track is the combination of the original "S" section and the small radius arc. The entrance speeds of each test track were designed to be relatively challenging compared to ordinary driving scenarios. The entrance speeds were 85 km/h for the 1st and 2nd test tracks, 75 km/h for the 3rd test track, and 65 km/h for the 4th test track.

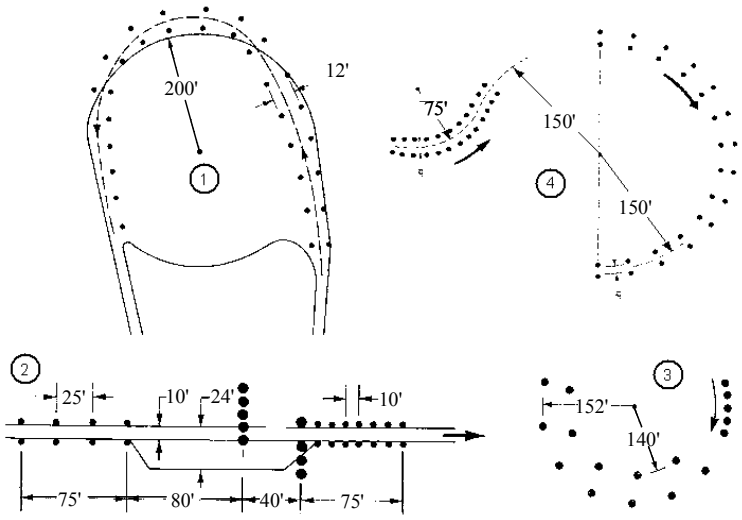

Fig. 17. Test tracks used for evaluating the anti-rollover control performance [30].

4.2 Control Gain Optimization

Before starting the optimization process, we need to select a performance index that can give us insightful evaluations of the anti-rollover control. Lin et al. [15,16,17] used Load-Transfer-Ratio (LTR), which was defined by Ervin [31], to evaluate their roll control system. LTR is defined as

$$LTR = \frac{F_L - F_R}{F_L + F_R} \tag{8}$$

where F_L is the sum of vertical forces at left tires. F_R is the sum of vertical forces at right tires. LTR ranges from –1 to 1. If the driver is driving straight, LTR is 0. For extreme conditions, the absolute LTR value can be equal to 1 when either right or left side of tires lifts off the ground. We chose the maximum value of absolute LTR (i.e., LTR_{max}) to be the performance index throughout the anti-rollover control design. The smaller the LTR_{max} is, the less the rollover danger. The optimization goal was to minimize the cost function LTR_{max}. The control gain K was optimized using the UMTRI driver model [32,33,34] and the test tracks listed in Section 4.1.

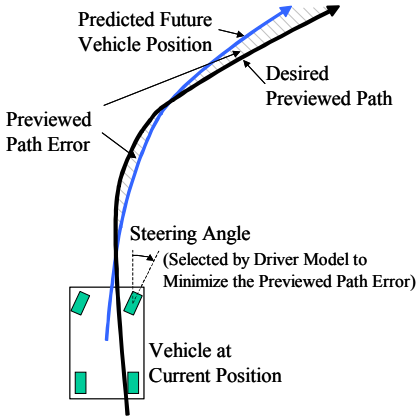

Fig. 18. Steering control strategy of UMTRI driver model [34].

Fig. 18 shows the steering control strategy of the UMTRI driver model. As can be seen from Fig. 18, the steering angle is selected such that the predicted future vehicle trajectory (dark solid line) will minimize the previewed path error (cross-shaded area). TruckSim has a built-in UMTRI driver model for the steer control [28]. Users can specify the desired path described in the global coordinates in TruckSim. The driver model will generate steering wheel angles to track the desired path. The algorithm flow of the UMTRI driver model in TruckSim is shown in Fig. 19.

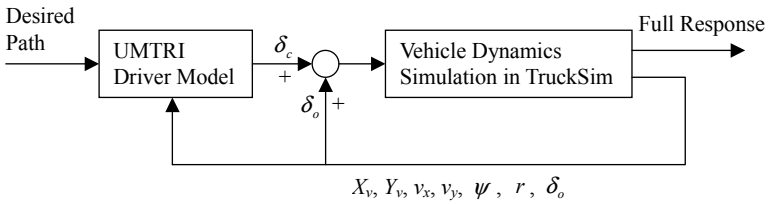

Fig. 19. Algorithm flow of the UMTRI driver model in TruckSim.

The driver model does not have knowledge of the full vehicle dynamics. It only has the information of the global coordinates of the center point of the front axle X_v and Y_v, longitudinal velocity v_x, lateral velocity v_y, yaw angle ψ, yaw rate r, and the steering due to the factors outside the direct control of the driver model δ_o (for example, roll steer). The driver model generates the steering by the following procedures: (1) it synthesizes the desired path over the preview time interval; (2) it minimizes previewed path errors over the preview time interval; (3) it calculates the optimal control steering δ_c; (4) it delays δ_c by a time delay τ_d to simulate the human muscular delay.

The procedure to minimize the cost function by each test track is described as follows: (1) the driver model drives the vehicle for different values (equally spaced) of the control gain; (2) a LTR_{max} value is recorded for each value; (3) searching the minimum LTR_{max} value to obtain the optimized control gain. The final optimized control gain K is then obtained by taking average of 4 control gains from 4 test tracks.

The LTR_{max} values for the 2nd test track is shown in Fig. 20. As can be seen from Fig. 20, only small gains reduced the LTR_{max} value compared to the vehicle without the anti-rollover control (i.e. K = 0). Higher gains did not reduce the LTR_{max} values. This did not agree with the analysis in Section 3.3. The slow actuator time constant (0.2 sec) might be the cause of this problem.

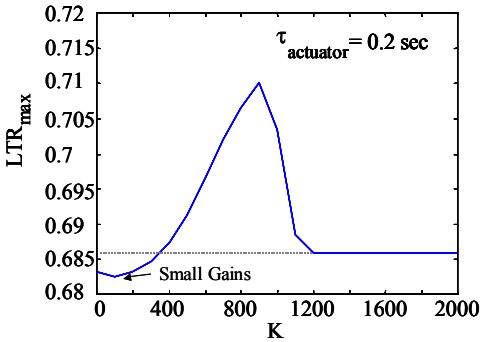

Fig. 20. LTR_{max} values of the 2nd test track.

Another faster actuator time constant was obtained from [35]. Fig. 21 shows the step response of the hydraulic brake model. As can be seen from Fig. 21, the time for the measured wheel cylinder pressure to reach 63% of the step pressure command is 0.15 sec.

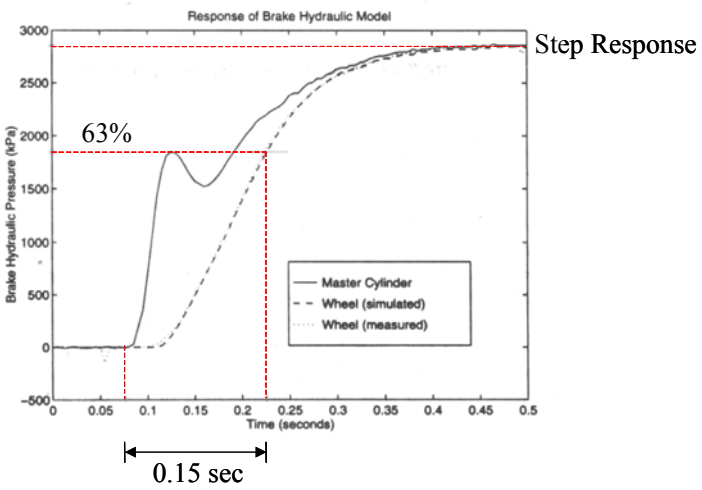

Fig. 21. Step response of Hydraulic Brake Model [35].

After we replaced the actuator time constant with 0.15 sec., we can get new LTR_{max} values for the 2nd test track (shown in Fig. 22). As can be seen from Fig. 22, higher gains did reduce the LTR_{max} values. This result agreed with the analysis in Section 3.3. We will use 0.15 sec. as the new time constant for the actuator dynamics throughout the control design. After the optimization process with the new actuator dynamics, the control gain K was 1320 kg-s^2-g (i.e.12950 kg-m).

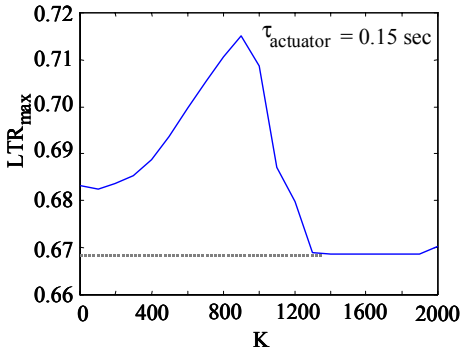

Fig. 22. LTR_{max} values of the 2nd test track with new actuator time constant.

4.3 Simulation Results

The performance of the proposed control system is compared with other threshold-based control algorithms in this subsection. Control gains of systems based on threshold values of lateral acceleration and roll angles were also optimized by following the procedures listed in Section 4.2. Threshold values of the lateral acceleration and roll angle were selected as 0.55g and 3 deg, respectively. The result is shown in Table 2.

Table 2. Average LTR_{max} values of control systems based on TTR, lateral acceleration, and roll angle.

Control / Feedback	Anti-rollover control based on			Without anti-rollover Control
	TTR	lateral acceleration	roll angle	
lateral acceleration	0.6702	0.6898	0.6989	0.8050
roll angle	0.6814	0.6915	0.6989	0.8050

In Table 2, the control system that is based on TTR with lateral acceleration as the feedback signal has the smallest average LTR_{max} values across the 4 test tracks. Table 2 also shows that

feeding back lateral acceleration has better performance than feeding back roll angle. We have decided to use the lateral acceleration instead of the roll angle as the feedback sign based on the previous control design. The result in Table 2 agreed with our decision in Section 3.3.

Before we conducted the human-in-the-loop experiment to validate the performance of the new control system, we used the UMTRI driver model to evaluate the closed-loop system. Fig. 23 shows the LTR_{max} of the closed-loop evaluations by using the UMTRI driver model (i.e., the UMTRI driver model drove the vehicles with and without anti-rollover control through 4 test tracks).

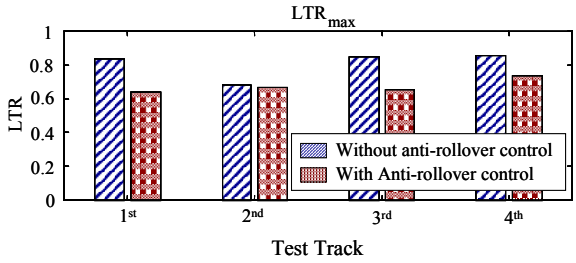

Fig. 23. LTR_{max} of closed-loop evaluations by UMTRI driver model.

As can be seen from Fig. 23, the anti-rollover control system can reduce the LTR_{max} values for the 1st, 3rd, and 4th test tracks significantly. The LTR_{max} for the 2nd test track was only reduced slightly. Since the LTR_{max} values were reduced in all test tracks, the closed-loop evaluation was determined to be satisfactory. The results of the human-in-the-loop experiment are presented in the following section.

5. HUMAN-IN-THE-LOOP EVALUATION

5.1 Driving simulator

The UM-Oakland driving simulator consists of two parts: the Virtual Vehicle System Simulator (VVSS) from Oakland University [25] (for generating the graphical interface) and a Jeep Cherokee TruckSim model from MSC (for simulating the vehicle dynamics). The experimental setup is shown in Fig. 24.

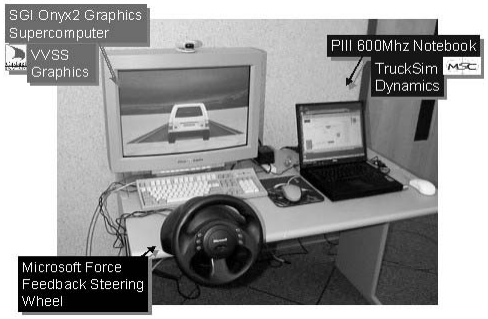

Fig. 24. Experimental setup of the UM-Oakland driving simulator.

VVSS is a simulation platform with an integrated network environment. VVSS was run on a SGI Onyx2 graphics supercomputer at the University of Michigan's Virtual Reality Lab. TruckSim and the TTR-based anti-rollover control algorithm were run on a Pentium III 600 MHz notebook computer. The communication between the Onyx2 and the notebook computer was through a 100BT Ethernet network. A Microsoft force feedback steering wheel was connected to the notebook computer as the steering interface. The force feedback feature of the steering wheel was turned on for more realistic driving feelings. It only worked as a torsional spring to generate the centering torque when drivers steered. The notebook computer took the test driver's steering input via the game port and sent it to TruckSim. The driver interacted with the driving simulator through a visualization monitor and the steering wheel. In order to simplify the experiment, the

driver was not allowed to brake or accelerate the vehicle. The test tracks in Section 4.1 were used again for the human-in-the-loop evaluation. The screen shots of those 4 test tracks are shown in Fig. 25.

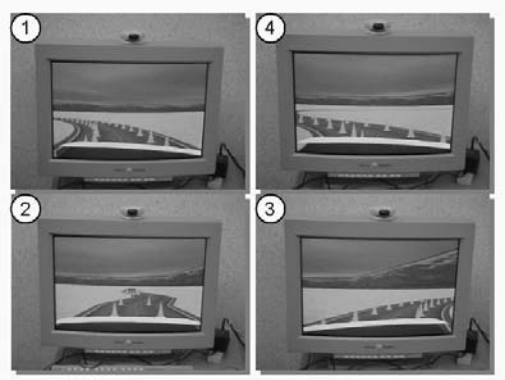

Fig. 25. Screen shots of the test tracks.

The direct measurement obtained from the steering wheel ranged from –1 to 1. The measurement was multiplied with a gain of 300 before being sent to TruckSim (i.e., the steering range was between –300 and 300 deg). In order to give the direct yaw moment control full capability of the available braking moment, there was no limitation imposed on the available braking moment on both front wheels. The maximum attainable braking moment never exceeded 2500 N-m that was limited by the maximum longitudinal braking force, because it was actually commanded by a sub-loop ABS for tracking the desired tire slip ratio.

5.2 Evaluation Results

36 test drivers participated in the experiment. Each driver was required to drive one vehicle. 18 drivers of the control group drove the vehicle equipped with the anti-rollover control system and another 18 drivers of the no control group drove the vehicle without the anti-rollover control system. The type of the vehicle was not revealed to the test driver until the end of the experiment. After all 36 test drivers finished the experiment, we averaged the LTR_{max} values of the no control group by each test track. Then we averaged the LTR_{max} values of the control group by each test track. The results are shown in Table 3. As can be seen from Table 3, the anti-rollover control can reduce the LTR_{max} values for the 1st, 3rd, and 4th test tracks significantly. However, it did not perform well for the 2nd test track. The LTR_{max} value for the 2nd test track was increased slightly by the anti-rollover control.

Table 3. Average LTR_{max} values of the control (with anti-rollover control) and no control (without anti-rollover control) groups.

	1st test track	2nd test track	3rd test track	4th test track
No control	0.8763	0.7809	0.8484	0.8865
Control	0.8168	0.8139	0.8107	0.7739

The histogram plot of the LTR_{max} values of the control and no control groups is shown in Fig. 26. Fig. 26 gave us more information than just the average values. We can understand the distribution of the test results. As can be seen from Fig. 26, the result agreed with Table 3. The numbers of drivers were denser around the average LTR_{max} values than the other values.

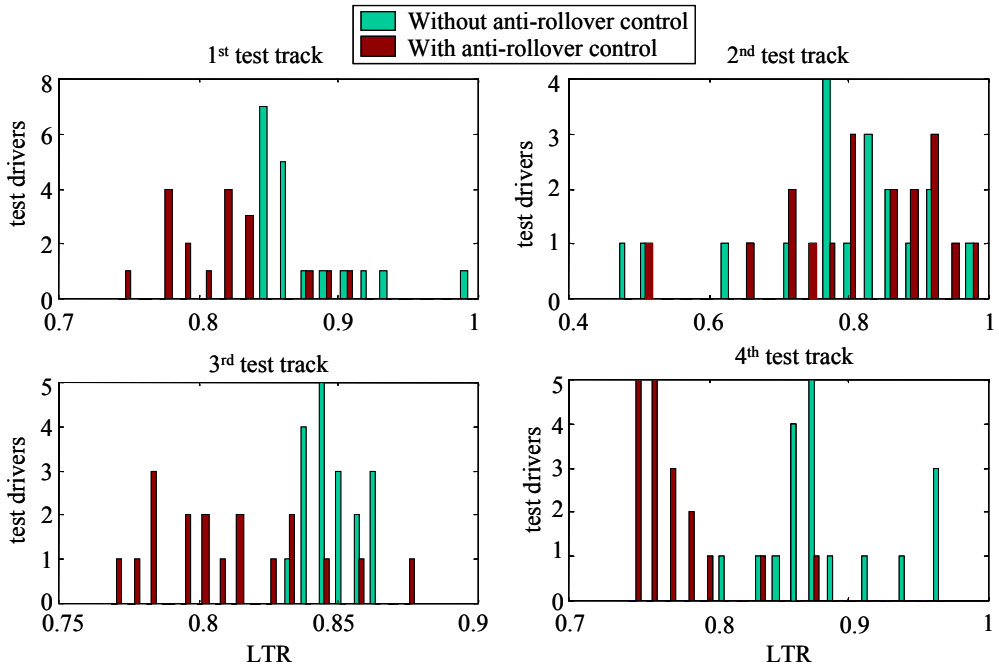

Fig. 26. Histogram plot of LTR_{max} values of the control (with anti-rollover control) and no control (without anti-rollover control) groups.

Because it was not clear why the proposed control algorithm did not perform well for the 2nd test track, we decided to study the steering angles of the control and no control groups. Fig. 27 shows average steering angles of control and no control groups. As can be seen from Fig. 27, the average steering angle of the control group was larger than that of the no control group, especially for the 2nd test track. Test drivers tended to steer more to compensate for the understeer effect of differential braking in order to follow the desired test track.

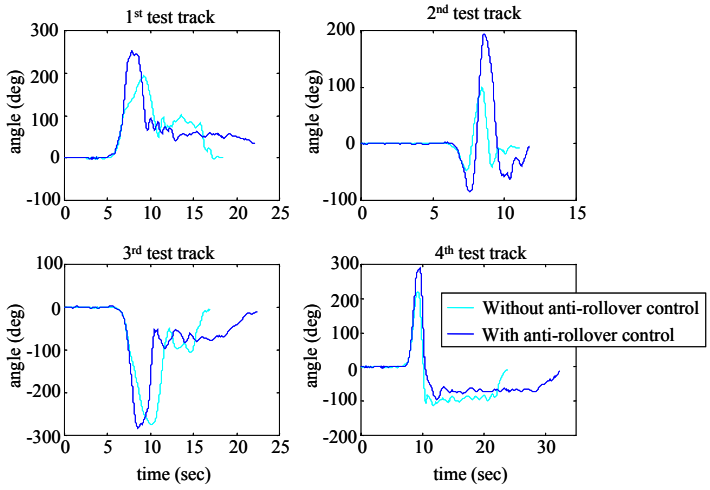

Fig. 27. Average steering angles of the control (with anti-rollover control) and no control (without anti-rollover control) groups.

An interesting observation from the experiment might be able to explain this result. The 2nd test track was designed for an obstacle avoidance maneuver. Two thirds of the test drivers of the no control group failed the test for the 1st and 2nd runs if they were trying to follow the test track tightly. The vehicle would either spin off or roll over. Therefore, they tended to steer less for the later runs to avoid spinning off or rollover and followed the test track loosely. However, none of

the test drivers of the control group failed the test for the 2nd test track. Neither spinning off nor rollover occurred. From Fig. 23, we found that the proposed control algorithm with the UMTRI driver model can only reduce the LTR_{max} value slightly for the closed-loop evaluation of the 2nd test track. Since the steering pattern of the real driver was much noisier than that of the UMTRI driver model, it degraded the performance of the proposed control algorithm and thus resulted in unsatisfactory consequence for the 2nd test track.

6. CONCLUSIONS AND FUTURE RESEARCH

6.1 Summaries and Conclusions

A high fidelity Jeep Cherokee model was built in the TruckSim dynamic simulation software environment to verify the performance of the proposed control algorithm. The Cherokee model in TruckSim was verified against the test data with lateral acceleration as high as 0.6 g. A 3DOF yaw-roll model with steering and direct yaw moment inputs was constructed by using the Cherokee parameters and tuned to match the test data. The root-locus technique was used to help design the feedback control of differential braking. After analyzing both lateral acceleration and roll angle feedback design, lateral acceleration was selected because it generated the desired and consistent root-locus pattern in both yaw and roll mode at all design speeds.

Because a driver closes the loop with the environment and the vehicle dynamics, the UMTRI driver model was used to help optimize the control gain. The control gain optimization was done by minimizing the maximum absolute LTR (LTR_{max}) values by each test track. During the optimization process, it was found that a faster actuator dynamics was necessary to satisfy the optimization goal for the test track of the obstacle avoidance maneuver (the 2nd test track). After the optimized control gain was achieved, closed-loop (the steering was specified by the driver model) evaluations were executed to examine the performance of the proposed anti-rollover control before conducting the human-in-the-loop experiment. The anti-rollover control system showed improved performance for all test tracks.

The human-in-the-loop experiment result showed that the anti-rollover control could improve the performance significantly for all test tracks, except for the test track of the obstacle avoidance maneuver. Because the steering pattern of the real driver was much noisier than that of the UMTRI driver model, it degraded the performance of the proposed control algorithm and thus resulted in larger load transfer for the obstacle avoidance maneuver.

6.2 Future Research

While this paper outlines the design, analysis, and evaluation of the anti-rollover control based on the TTR metric, there are still many open issues:

I. The proposed anti-rollover control algorithm for SUVs can improve the performance significantly for all the test scenarios we have studied, except for the 2nd test track (obstacle avoidance maneuver). It might be possible that a more sophisticated control design could demonstrate superior performance in all cases. For example, proportional-derivative (PD) control, optimal control, and nonlinear control are all possible techniques for the control design.

II. For the human-in-the-loop experiments, a motion-base driving simulator could be used to provide complete visual-motion-haptic-audio cues to drivers. The redesign and analysis of the active safety system under these more advanced driving simulators is a natural follow-up task for this paper.

III. The TTR-based anti-rollover control algorithm is proposed in this paper to solve the on-road, untripped rollover problem. However, the on-road, untripped rollover is a small portion of rollover accidents, and is much simpler than the tripped rollover. Considering the tripping mechanism, it can be a very challenging task to solve the tripped rollover problem.

Vehicle System Dynamics, Vol 36, No.4-5, November 2001, pp.359-389

ACKNOWLEDGEMENT

This research is supported by the U.S. Army TARDEC under the contract DAAE07-98-C-R-L008. The authors wish to thank Dr. Riley Garrott and Mr. Paul Greiger of VRTC for supplying the vehicle test data, Dr. Michael Sayers and Dr. Stephen M. Riley of Mechanical Simulation Corporation for technical supports and customizations of TruckSim, Dr. G. Edzko Smid and Prof. Ka C. Cheok of Oakland University for helping implement the UM-Oakland driving simulator at University of Michigan.

REFERENCE

1. National Highway Traffic Safety Administration: Traffic Safety Facts 1993-1998: A Compilation of Motor Vehicle Crash Data from the fatality Analysis Reporting System and the General Estimates System. 1994-1999.

2. U.S. Department of Transportation, Office of Public Affairs: DOT Requires Upgraded Rollover Warning Label for Sports Utility Vehicles. Press Releases No. NHTSA 8-99, March 5, 1999.

3. National Highway Traffic Safety Administration: DOT Announces Proposal to Add Rollover Ratings To Auto Safety Consumer Information Program. NHTSA Now, Vol.6, No.7, June 19, 2000.

4. Woodrooffe, J.H.F., "Practical Concepts In Heavy Truck Rollover Accident analysis," Heavy Vehicle Rollovers Conference, April 29-30, 1993, Atlanta, Ga.

5. Rakheja, S. and Pichè, A., "Development of Directional Stability Criteria for an Early Warning Safety Device," SAE Paper No. 902265, 1990.

6. Preston-Thomas, J. and Woodrooffe, J.H.F., "A Feasibility Study of a Rollover Warning Device for Heavy Trucks," Transport Canada Publication No. TP 10610E, September 1990.

7. Freedman, M., Olson, P.L., and Zador, P.L., "Speed Actuated Rollover Advisory Signs for Trucks on Highway Exit Ramps," Insurance Institute for Highway Safety and University of Michigan Transportation Research Institute, December 1992.

8. McGee, H., Joshua, S., Hughes, W., Strickland, R., Bareket, Z., and Fancher, P., "Feasibility of An Automatic Truck Warning System," FHWA-RD-93-039, June1993.

9. Strickland, R. and McGee, H., "Evaluation of Prototype Automatic Truck Rollover Warning Systems," FHWA-RD-97-124, 1997.

10. Ervin, R.D., Winkler, C.B., Fancher, P.S., Hagan, M., Krishnaswami, V., Zhang, H., Bogard, S., and Karamihas, S. "Cooperative Agreement to Foster the Deployment of a Heavy Vehicle Intelligent Dynamic Stability Enhancement System," University of Michigan Transportation Research Institute, Interim report, NHTSA – U.S. DOT Contract No. DTNH22-95-H-07002, January 1998.

11. Chen, B. and Peng, H.: A Real-time Rollover Threat Index for Sports Utility Vehicles. Automatic Control Conference, June 1999.

12. Chen, B. and Peng, H.: Rollover Warning For Articulated Vehicles Based on A Time-To-Rollover Metric. ASME International Mechanical Engineering Conference and Exhibition, November 1999.

13. Furleigh, D.D., Vanderploeg, M.J., and Oh, C.Y.: Multiple Steered Axles for Reducing the Rollover Risks of Heavy Articulated Trucks. SAE Paper No. 881866, 1988.

14. Dunwoody, A.B.: Active Roll Control of a Semi-Trailer. SAE Paper No. 933045, 1993.

15. Lin, R.C.: An Investigation of Active Roll Control for Heavy Vehicle Suspensions. Ph.D. Thesis, Cambridge University Engineering Department, 1994.

16. Lin, R.C., Cebon, D., and Cole D.J.: Active Roll Control of Articulated Vehicles. VSD, Vol. 26, No. 1, pp. 17-43, 1996.

17. Lin, R.C., Cebon, D., and Cole D.J.: Optimal roll-control of a single-unit lorry. J. Auto. Eng., Proc. ImechE, D05294, pp. 45-55, 1996.

18. Sampson, D.J.M. and Cebon, D.: An Investigation of Roll Control System Design for Articulated Heavy Vehicles. AVEC'98, Paper No. 9836815, 1998.

19. Parsons, K., Pask, M., and Burdock, W.: The Development of ACE for Discovery II. SEA-paper No. 00PC-60, 1998.

20. Konik, D., Bartz, R., Barnthol, F., Bruns, H., and Wimmer, M.: Dynamic Drive – the New Active Roll Stabilization System from the BMW Group – System Description and Functional Improvements. AVEC 2000, 5th International Symposium on Advanced Vehicle Control, August 2000.

21. Palkovics, L., Semsey, A. and Gerum, E.: Roll-Over Prevention System for Commercial Vehicles – Additional Sensorless Function of the Electronic Brake System. AVEC'98, Paper No. 9837409, 1998.

22. Palkovics, L., Semsey, A. and Gerum, E.: Roll-Over Prevention System for Commercial Vehicles – Additional Sensorless Function of the Electronic Brake System. Vehicle System Dynamics, Vol.32, No.4, pp.285-297, 1999.

23. Wielenga, T.J.: A Method for Reducing On-Road Rollovers – Anti-Rollover Braking. SAE Paper No. 1999-01-0123, 1999.

24. Wielenga, T. J. and Chace, M. A. "A study of rollover prevention using anti-rollover braking. SAE Paper No. 2000-01-1642, 2000.

25. Smid, G.E.: Virtual Vehicle Systems Simulation: A Modular Multi-CPU approach in Real-Time. Ph.D. dissertation, Oakland University, Rochester, Michigan, 1999.

26. Peng, H.: Lecture Notes for ME542: Vehicle Dynamics", Mechanical Engineering Department, University of Michigan, 1996.

27. Salaani, M.K., Guenther, D.A., and Heydinger, G.J.: Vehicle Dynamics Modeling for the National Advanced Driving Simulator of a 1997 Jeep Cherokee. SAE Paper No. 1999-01-0121.

28. Mechanical Simulation Corporation: TruckSim User Reference Manual. February 1999.

29. Koibuchi, K., Yamamoto, M., Fukada, Y., and Inagaki, S.: Vehicle Stability Control in Limit Corning by Active Brake. SAE Paper No. 960487.

30. Rice, R.S., Dell'Amico, F., and Rasmussen, R.E.: Automobile Driver Characteristics – The Man-Off-The-Street. SAE Paper No. 760777.

31. Ervin, R.D. and Guy, Y.: The influence of weights and dimensions on the stability and control of heavy-duty trucks in Canada. Volume I - technical report. Final Report, Michigan University, Ann Arbor, Transportation Research Institute, Report No. UMTRI-86-35/I, 1986.

32. MacAdam, C.C.: An optimal preview control for linear systems. Journal of Dynamic Systems, Measurement and Control, Vol. 102, pp. 188-190, September 1980.

33. MacAdam, C.C.: Application of an optimal preview control for simulation of closed-loop automobile driving. IEEE Transactions on Systems, Man and Cybernetics, Vol. SMC-11, No. 6, pp. 393-399, June 1981.

34. MacAdam, C.C.: Mathematical Modeling of Driver Steering Control at UMTRI - An Overview. UMTRI Research Review, Vol. 20, No. 1, July-Aug 1989, pp. 1-13, 1989.

35. Hedrick, J.K., Gerdes, J.C., Maciuca, D.B., and Swaroop, D.: Brake system modeling, control and integrated brake/throttle switching: phase I. California University, Berkeley, Department of Mechanical Engineering, Calif. PATH Research Report No. UCB-ITS-PRR-97-21, 1997.

APPENDIX 1

Detailed descriptions of Eq.(1):

$$m = m_R + m_{NR} \qquad Y_\beta = -\left(C_{\alpha f} + C_{\alpha r}\right)$$

$$Y_r = \frac{bC_{\alpha r} - aC_{\alpha f}}{u_0} \qquad Y_\phi = C_{\alpha r}\frac{\partial \delta_r}{\partial \phi} + C_{\gamma f}\frac{\partial \gamma_f}{\partial \phi}$$

$$Y_\delta = C_{\alpha f} \qquad N_\beta = bC_{\alpha r} - aC_{\alpha f}$$

$$N_r = -\frac{a^2 C_{\alpha f} + b^2 C_{\alpha r}}{u_0} \qquad N_\phi = aC_{\gamma f}\frac{\partial \gamma_f}{\partial \phi} - bC_{\alpha r}\frac{\partial \delta_r}{\partial \phi}$$

$$N_\delta = aC_{\alpha f} \qquad L_\phi = m_R g h - K_R$$

$$L_p = -c_R \qquad I_x = \left(I_{xx}\right)_R + m_R h^2 - 2\theta_R\left(I_{xz}\right)_R + \theta_R^2\left(I_{zz}\right)_R$$

$$I_{xz} = m_R hc - \left(I_{xz}\right)_R + \theta_R\left(I_{zz}\right)_R \qquad I_z = \left(I_{zz}\right)_R + \left(I_{zz}\right)_{NR} + m_R c^2 + m_{NR} e^2$$

Parameters used in Eq.(1):

m_R : Rolling sprung mass, 1663 kg.

m_{NR} : Non-rolling unsprung mass, 324.935 kg.

θ_R : Inclination angle of the roll axis point down, 0.0873 rad.

a : Distance from the vehicle CG to the front axle, 1.1473 m.

b : Distance from the vehicle CG to the rear axle, 1.4307 m.

c : Distance fron the CG of m_R to point O (shown in Figure 4.5), 0.4214 m.

e : Distance fron the CG of m_{NR} to point O, 2.1566 m.

g : Gravity, 9.81 m/s^2.

h : Distance from the CG of m_R to the roll axis, 0.306 m.

$C_{\alpha f}$: Front tire cornering stiffness, 59496 N/rad.

$C_{\alpha r}$: Rear tire cornering stiffness, 109400 N/rad.

$\frac{\partial \delta_r}{\partial \phi}$: Partial derivative of the roll induced steer at the rear axle, 0.07.

$\frac{\partial \gamma_f}{\partial \phi}$: Partial derivative of the camber thrust at the front axle, 0.8.

$C_{\gamma f}$: Camber thrust coefficient at the front axle, 2038.8 N/rad.

K_R : Roll stiffness, 56957 N-m/rad.

c_R : Roll damping coefficient, 3495.7 N-m-sec/rad.

$(I_{xx})_R$: Moment of inertia about the x-axis of the rolling sprung mass, 602.8220 kg-m^2.

$(I_{xz})_R$: Product of inertia about the x-z axes of the rolling sprung mass, 89.9914 kg-m^2.

$(I_{zz})_R$: Moment of inertia about the z-axis of the rolling sprung mass, 2163.7 kg-m^2.

$(I_{zz})_{NR}$: Moment of inertia about the z-axis of the non-rolling unsprung mass, 540 kg-m^2.